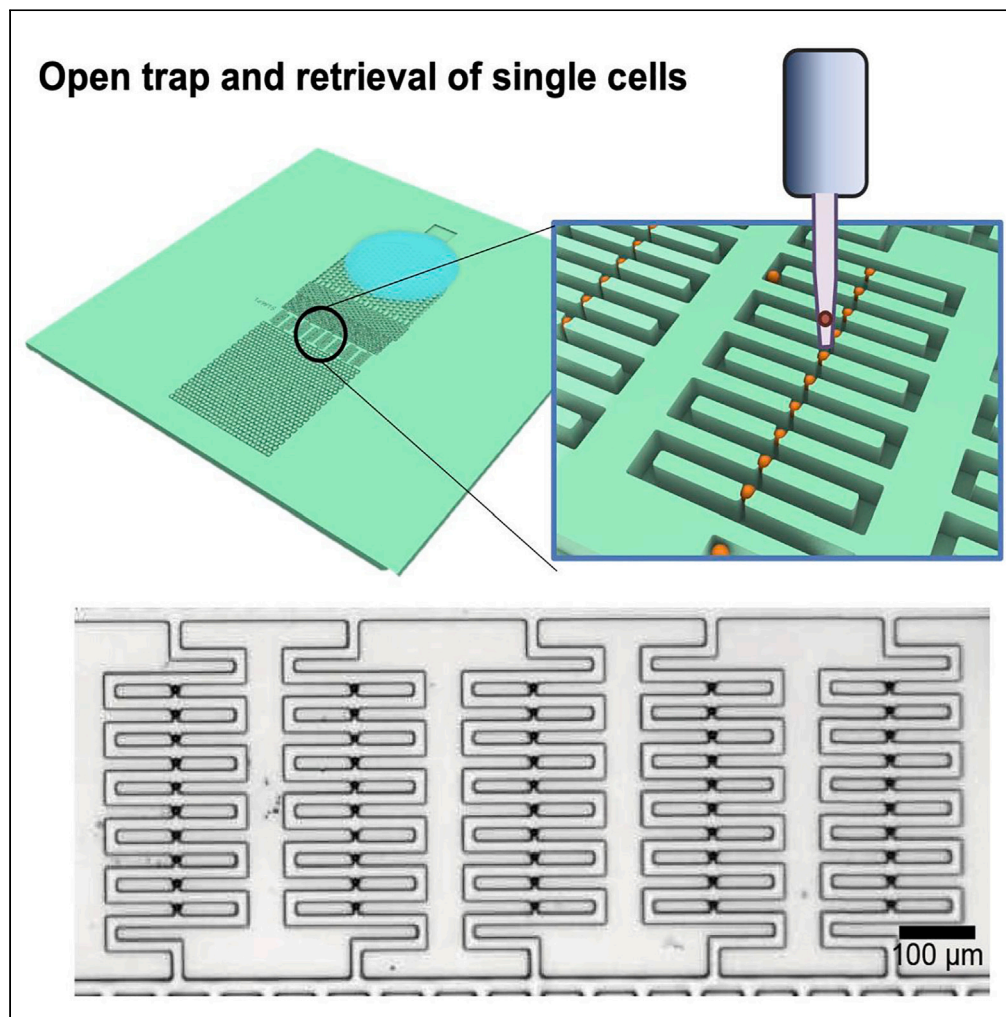


Article

Single-cell trapping and retrieval in open microfluidics



Tomoki Murakami,
Hiroto Teratani,
Dai'ichiro Aoki,
Masao Noguchi,
Mamiko Tsugane,
Hiroaki Suzuki

suzuki@mech.chuo-u.ac.jp

Highlights

Hydrodynamic single-cell trapping was realized in an open microfluidics platform

Hydrophilic treatment only inside open narrow channel was performed

Open microfluidics platform allowed single cell picking after trapping

Murakami et al., iScience 26,
108323
November 17, 2023 © 2023 The
Authors.
[https://doi.org/10.1016/
j.isci.2023.108323](https://doi.org/10.1016/j.isci.2023.108323)

Article

Single-cell trapping and retrieval
in open microfluidics

Tomoki Murakami,^{1,4} Hiroto Teratani,^{1,4} Dai'ichiro Aoki,² Masao Noguchi,³ Mamiko Tsugane,¹
and Hiroaki Suzuki^{1,5,*}

SUMMARY

Among various single-cell analysis platforms, hydrodynamic cell trapping systems remain relevant because of their versatility. Among those, deterministic hydrodynamic cell-trapping systems have received significant interest; however, their applications are limited because trapped cells are kept within the closed microchannel, thus prohibiting access to external cell-picking devices. In this study, we develop a hydrodynamic cell-trapping system in an open microfluidics architecture to allow external access to trapped cells. A technique to render only the inside of a polydimethylsiloxane (PDMS) microchannel hydrophilic is developed, which allows the precise confinement of spontaneous capillary flow in the open-type microchannel with a width on the order of several tens of micrometers. Efficient trapping of single beads and single cells is achieved, in which trapped cells can be retrieved via automated robotic pipetting. The present system can facilitate the development of new single-cell analytical systems by bridging between microfluidic devices and macro-scale apparatus used in conventional biology.

INTRODUCTION

Over the past decade, methodologies for single-cell analysis have increased exponentially.^{1–3} In particular, droplet-based technologies have expanded rapidly, beginning with early digital gene expression profiling methods, followed by the commercialization of single-cell comprehensive RNA sequencing (scRNA-seq).^{4–6} In droplet-based methods, a single cell and barcode DNA are co-encapsulated and tagged in a small, closed space; subsequently, the barcoded cDNA library is extracted in bulk for further analysis using a next-generation sequencer. Although this method is extremely effective for revealing expression profiles of single cells, it is less flexible for multimodal analysis because of the difficulty in adding reagents and imaging after the initial encapsulation step.

In applications such as single-cell imaging, cell culture, drug assays, screening, and other assays involving more complex reagent manipulation, single cells could be isolated and transferred to conventional well plates for microscopic observations and assaying using existing kits.^{7,8} A simple solution is to disperse cells over a substrate at an extremely low concentration and then retrieve and transfer them to a well plate. However, the random positioning of cells renders their industrial use challenging; picking cells from random locations requires sophisticated image processing, identification, and positioning. Moreover, this method may cause neighboring cells to be accidentally aspirated. To facilitate robotic imaging and the picking of numerous single cells, single cells should be arranged in an array on a flat substrate. The simplest method is to create single-cell arrays via vertical sedimentation in microwells,^{9,10} which is a technique typically employed in industry and basic research owing to its simplicity and ease of operation.^{11,12} However, the entry of cells into wells is typically stochastic, and a 100% arraying efficiency is difficult to achieve.

To date, various deterministic lateral cell arraying methods have been investigated and developed using hydrodynamic trapping,^{13–15} with the earliest studies conducted by Di Carlo et al. in 2006¹⁶ and Tan et al. in 2007.¹⁷ Trapping efficiencies of approximately 100% have been realized for many devices. However, the industrial applications of these devices are limited. One of the possible limitations is that, whereas microwells can be opened at the top, thus allowing access to reagents and capillaries for picking, most hydrodynamic trapping devices are constructed based on a closed microchannel driven by syringe pumps or pressure pumps. Therefore, additional operations after single-cell isolation are difficult, and downstream protocols must be integrated within the same microchannel system. Fluidigm has realized multiple operations (cell lysis and addition of PCR reagents) after microfluidic trapping using an integrated fluidic circuit (IFC) with built-in pneumatic valves.¹⁸ However, the entire system and the IFC chip are complicated and expensive.

Open microfluidic platforms are expected to ease the integration of microfluidic devices and macroscale systems by allowing direct access to additional reagents and manual or robotic pipettes.^{19–21} In particular, fluid control techniques using spontaneous capillary flow (SCF) only

¹Department of Precision Mechanics, Graduate School of Science and Engineering, Chuo University, Kasuga 1-13-27, Bunkyo-ku, Tokyo 112-8551, Japan

²Aeternus Co., Ltd, Minamidai 2-1-14, Fujimino, Saitama 356-0036, Japan

³Caravell Co., Ltd, Surugadai 1-29-39, Funabashi, Chiba 273-0862, Japan

⁴These authors contributed equally

⁵Lead contact

*Correspondence: suzuki@mech.chuo-u.ac.jp

<https://doi.org/10.1016/j.isci.2023.108323>



require an extremely simple setup. By employing geometric confinement or spatial patterns of fluid wetting on a substrate, a microscale flow in the desired paths can be generated. Although the mechanism of SCF has been investigated comprehensively,^{20,22,23} its application is still limited despite its simplicity.^{24–26} SCF-based microfluidic systems have been primarily demonstrated via microchannels on the order of millimeters to submillimeters, although applications for single-cell analysis require a spatial resolution of 10 μm . This is likely because precise flow control comparable to the size of cells has been difficult to achieve in open microchannels. As a representative example, size-based separation of cells using deterministic lateral displacement has been demonstrated in an open microfluidics platform.²⁷ Another group developed an open-type stochastic cell-trapping device for a selective cell-picking apparatus for commercial use.²⁸ However, to the best of our knowledge, deterministic hydrodynamic single-cell trapping has not yet been achieved.

In this study, we show that precise fluid control in a single-cell trapping architecture can be realized by performing hydrophilic treatment only on the inside of open channels measuring several tens of micrometers. We demonstrate single-bead and single-cell trapping by depositing a water suspension, after which trapped cells can be retrieved via manual or robotic capillary pipette aspiration.

RESULTS AND DISCUSSION

Testing SCF in narrow channels

Open microfluidics are based on the spontaneous wetting of the inner walls of channels. This phenomenon is termed as SCF. Based on theoretical prediction, SCF occurs when the channel wall is hydrophilic (contact angle $<90^\circ$) and the cross-sectional shape of the channel satisfies the following equation²⁰:

$$\frac{p_f}{p_w} < \cos \theta, \quad (\text{Equation 1})$$

where p_w and p_f represent the wetted perimeter (the length of the liquid–solid interface) and free perimeter (the length of the air–liquid interface) of the channel cross-section, respectively. Therefore, for an open channel with a rectangular cross-section (width W and height H), the SCF of a liquid with contact angle θ occurs when Equation 2 is satisfied.

$$\frac{W}{W+2H} < \cos \theta. \quad (\text{Equation 2})$$

To date, SCFs have been demonstrated experimentally and analyzed theoretically, but most experimental studies were performed based on relatively large channel dimensions, i.e., typically several hundreds of micrometers. For single-cell trapping, SCFs must be realized in a flow path whose size is comparable to that of cells (10–50 μm). Practical problems may arise under such a regime. Equation 2 theoretically predicts that SCF occurs in trenches with relatively large aspect ratios (large H). Ideally, although the surface wettability is the same inside and outside the channel, the flow should be confined to only the inside of the channel because of the pinning effect at the corners on the surface of the rectangular trench. However, the corner angle of actual micro-trenches cannot be ideal 90° . If the outside of the channel (device surface) is hydrophilic, then the solution tends to spread out and thus will not be introduced efficiently into the channel. Therefore, in this study, we employed a strategy in which only the inner walls (bottom and side walls) of a top-side-opened polydimethylsiloxane (PDMS) microchannel are treated as hydrophilic, whereas the outer surface of the channel (native PDMS) remains hydrophobic. This structure strengthens the pinning effect at the corner of the rectangular channel, thus promoting liquid confinement within the channel.

The procedure for the hydrophilic treatment of the inside of an open PDMS channel is shown in Figure 1A. First, the microchannel side of the PDMS plate, in which through-holes were opened at both ends of the channel, was temporarily made hydrophilic by applying O_2 plasma. Additionally, another native PDMS flat plate was prepared. The flat plate was not treated with O_2 plasma to prevent covalent bonding. Subsequently, the plates were laminated together via gentle pressing using a finger. Next, an aqueous solution containing an amphiphilic polymer (either 1%v/v Pluronic F-68 surfactant or polyvinyl alcohol (PVA) solution) was introduced into the channel through a hole. We tested these two polymer solutions because they have been previously used to hydrophilize PDMS surfaces.^{29–31} These solutions flowed spontaneously into the channel (Video S1) owing to the hydrophilic nature of the channel walls. After the inside of the channel was completely filled, it was incubated for 30 min, and the solution was removed from the opposite hole via vacuum suction. Subsequently, the PDMS flat plate was peeled off and the channel device was baked on a hot plate (20 min, 120°C) with the channel side down to promote drying. After removing the device from the coverglass and flipping it, the inlets/outlets of the open channel device were covered with another PDMS plate from the backside; thus, the device was ready for use. For long-term storage, the channel surface was protected with Scotch tape.

The open channel used for the SCF test was designed as shown in Figure 1B. This channel comprised three main sections: 1) a drop section, 2) an open-channel section, and 3) a flow-drive section. The drop section is the area in which the sample is applied. This section was designed to be wide such that it can function as a reservoir for the bulk sample. A large number of micropillars (width: 50 μm , spacing: 50–10 μm) was placed to initiate SCF such that the sample would be transported into the channel section. The single-track channel at the channel section was designed such that the distance from the rectangular mark at the center of each meandering section to the next mark was 1 mm and the total length was 20 mm (Figure 1C). The flow drive section is a wide and long section with a large number of micropillars. Hence, the propagating front of SCF is maintained at a nearly constant velocity for a certain duration (typically several tens of seconds to a few minutes depending on the velocity). At the same time, drying at the channel section was suppressed because a new solution was supplied due to the flow (this section is unnecessary for the SCF test but necessary for hydrodynamic trapping experiments). A photograph of the device is shown in Figure 1D.

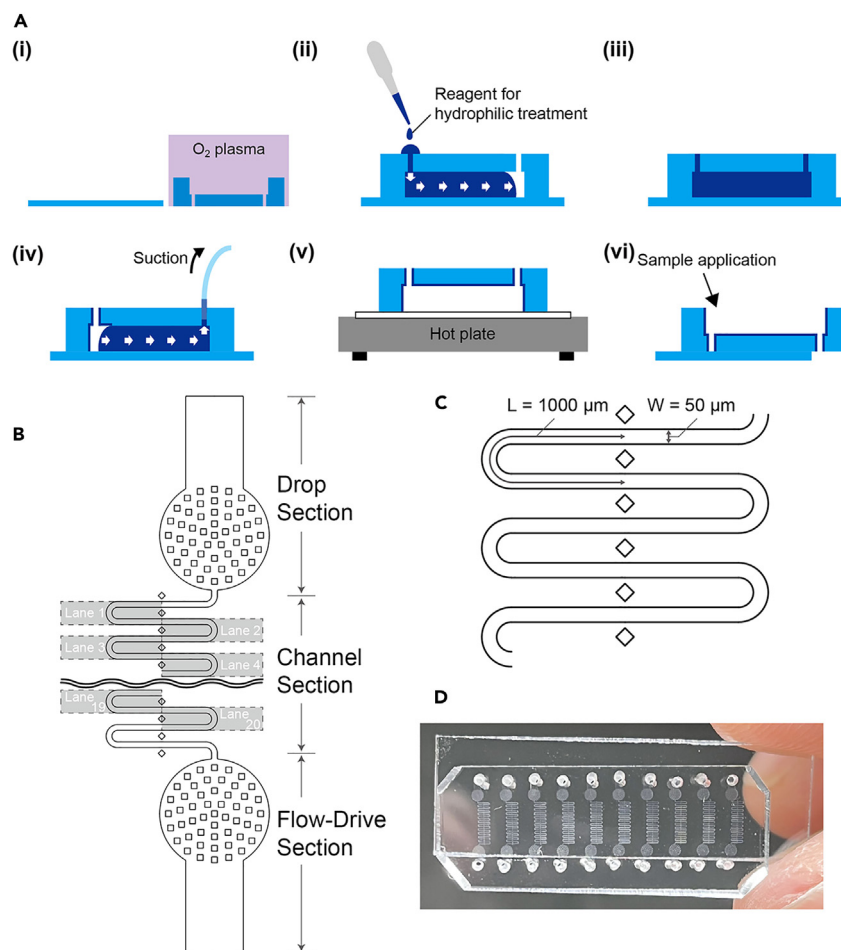


Figure 1. Fabrication process and design of the open microchannels

(A) Procedure for hydrophilic treatment of inner surfaces of PDMS open microchannel. (i) Oxygen plasma treatment of the channel. (ii) Introduction of hydrophilic coating reagent after closing the channel. (iii) Incubation at RT. (iv) Suction of reagent. (v) Baking. (vi) SCF test.

(B) Design of open microchannel for SCF test.

(C) Close-up view of the channel region.

(D) Overview of the device. PDMS plate was attached to the backside of the channel device to close the hole used to introduce the surface treatment reagent.

The effects of the dimensions of the channel cross-section and hydrophilic treatment agents were investigated. Open-channel devices with a rectangular cross-section, a constant width ($W = 50 \mu\text{m}$), and varying heights H (16, 42, and $78 \mu\text{m}$) were fabricated. The differences between PVA and F-68 surfactant treatments were investigated. When $1 \mu\text{L}$ of water (or aqueous solution) was deposited onto the drop section, the front of the water propagated between the pillars and entered the channel. The time points at which the advancing front passed the marks were extracted from the movie recorded at 40 fps.

In the case of the channel treated with 1% PVA, the speed of the moving front of pure water was slow (Video S2, real-time movie), with velocities and corresponding flow rates ranging from 0.05 to 0.2 mm/s and 0.1 to 1 nL/s, respectively (Figure S1). Meanwhile, it was much faster in the channel treated with F-68 Pluronic surfactant (amphiphilic diblock copolymer), with velocities and corresponding flow rates up to $\sim 6 \text{ mm/s}$ and $\sim 25 \text{ nL/s}$, respectively. Note that, as the front of the SCF proceeds, the velocity and the flow rate gradually decrease because the viscous drag of fluid pulling behind the front increases. Although the simple criteria for the occurrence of SCF are expressed by Equation 1, the propagation dynamics of the SCF (the distance traveled by the front, z) is predicted in the viscous regime of the Lucas–Washburn–Rideal law (LWR) as a function of time t , i.e.,^{20,23}

$$z = \sqrt{\frac{\gamma}{\mu}} \sqrt{\cos \theta^*} \sqrt{2\bar{\lambda}t} = \beta\sqrt{t}, \quad (\text{Equation 3})$$

where $\bar{\lambda}$ is the average friction length along the walls in a cross-section, γ the surface tension of the fluid in air, μ the viscosity of the sample fluid, and θ the generalized Cassie angle. This law states that z increases proportionally to the square root of t . Based on this theory, we plotted z obtained from the experimental observation against \sqrt{t} . The SCF test was repeated thrice for each condition (Figure 2A). The results fitted

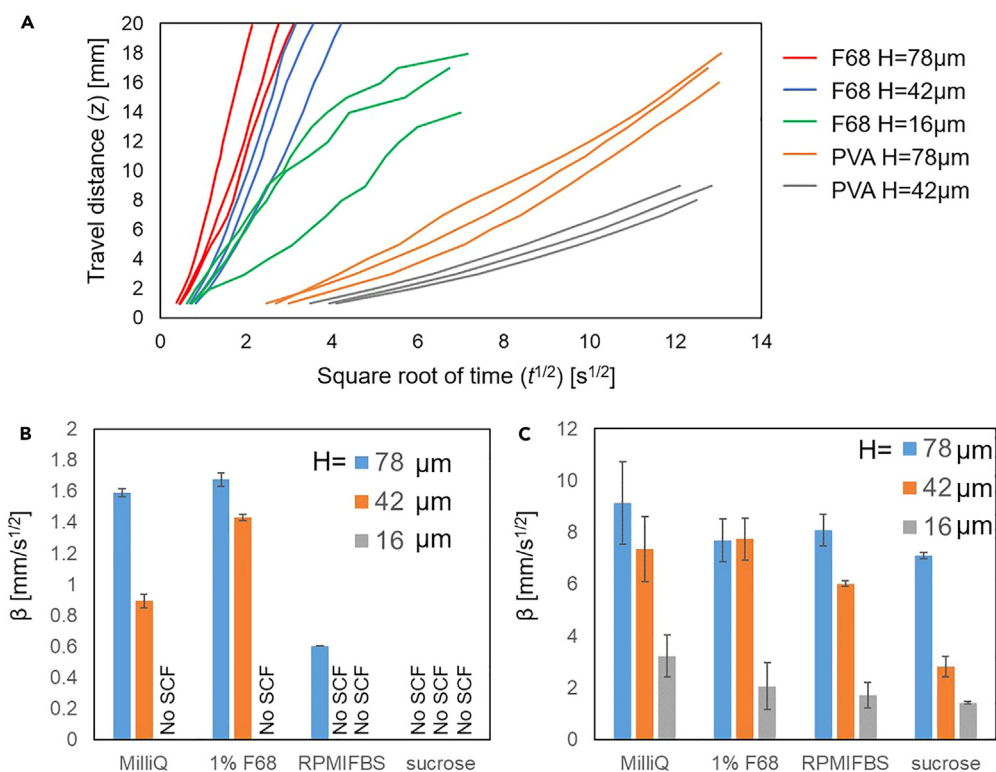


Figure 2. Performance tests of the spontaneous capillary flow

(A) Travel distance of advancing front of SCF in open microchannels ($W = 50 \mu\text{m}$) with various H and hydrophilic treatments. Each set of three lines with identical colors shows the result of triplicated experiments.

(B) Plot of β values obtained using Equation 2 for PVA-treated open channels and various solutions.

(C) Plot of β values obtained using Equation 2 for F68-treated open channels and various solutions. Error bars in all panels represent standard deviations in triplicated experiments.

the theory fairly well, with a linear increase in z against \sqrt{t} (Figure S2), although in some cases, the data plot deviated from the line at the later section of the channel. Under the same treatment (F-68 or PVA), the deeper channel yielded a faster SCF that traveled further within the same period, which is consistent with the LWR law. Notably, the F-68 treatment yielded an SCF that was significantly faster than that afforded by the PVA treatment. For example, the SCF traveled a distance of 20 mm (end of the test channel) within 5 s under F-68, whereas more than 2 min was required under PVA. SCF did not occur in the PVA-treated channels at $H = 16 \mu\text{m}$.

The progression of the SCF also varied depending on the type of flowing solution. The same SCF tests were performed for Milli-Q water, an aqueous solution containing 1%v/v F-68 surfactant, a cell culture medium (RPMI-FBS), and 25% sucrose solution with high viscosity (~ 2.5 cP). Subsequently, the linear region was fitted via the least-squares method using Equation 3 to obtain the constant term $\beta = \sqrt{\frac{z}{t}} \sqrt{\cos \theta^*} \sqrt{2\lambda}$ (Figures 2B and 2C). Larger β values represent faster SCFs. Under PVA treatment, Milli-Q water and F-68 solution flowed slowly in the 78 and 42 μm channels but not in the 16 μm channel. The medium flowed only at $H = 78 \mu\text{m}$, and no flow of sucrose solution occurred at any channel size (Figure 2B). However, under F68 treatment, the F68 solution and medium flowed at the same rate as Milli-Q water, although the flow rate of sucrose was lower, which might be because β is proportional to $-1/2$ power of viscosity.

The static contact angle measurements showed similar values for the F-68-treated and PVA-treated PDMS surfaces (F68, $22.8^\circ \pm 2.9^\circ$; PVA, $28.3^\circ \pm 2.6^\circ$; native PDMS, $97.6^\circ \pm 1.3$) (Figure S3A). Therefore, the difference in SCF velocity was not due to the F-68-treated surface being more hydrophilic. Thus, we hypothesized that the difference was due to the dynamic wetting properties. The measurement of the advancing contact angle via the extension/contraction method revealed that the F-68-treated surface wetted significantly more easily in all the solutions tested (Figure S3B). The dynamic contact angle is affected by surface roughness and uniformity.³² Thus, the difference in the speed of SCF might be because the F-68-treated surface was uniform and smooth at the molecular level.

In addition, the baking time after F68 treatment affected the SCF. For device fabrication, we set 20 min as the standard baking time because the channel should be dried to obtain reproducible SCF results. However, the SCF progressed faster in both solutions when the channel was used after the soaking/aspiration and removal of the lid (Figure S4A). The β value decreased slightly as baking time increased but remained almost constant above 20 min (Figure S4B). This is likely because the moist polymeric surface had better wetting dynamics and water was completely dried after 20 min of baking. The open channel baked for 20 min resulted in an SCF even after one week of storage at a rate comparable to that used on the same day as the treatment. We employed a baking time of 10–20 min in all subsequent experiments.

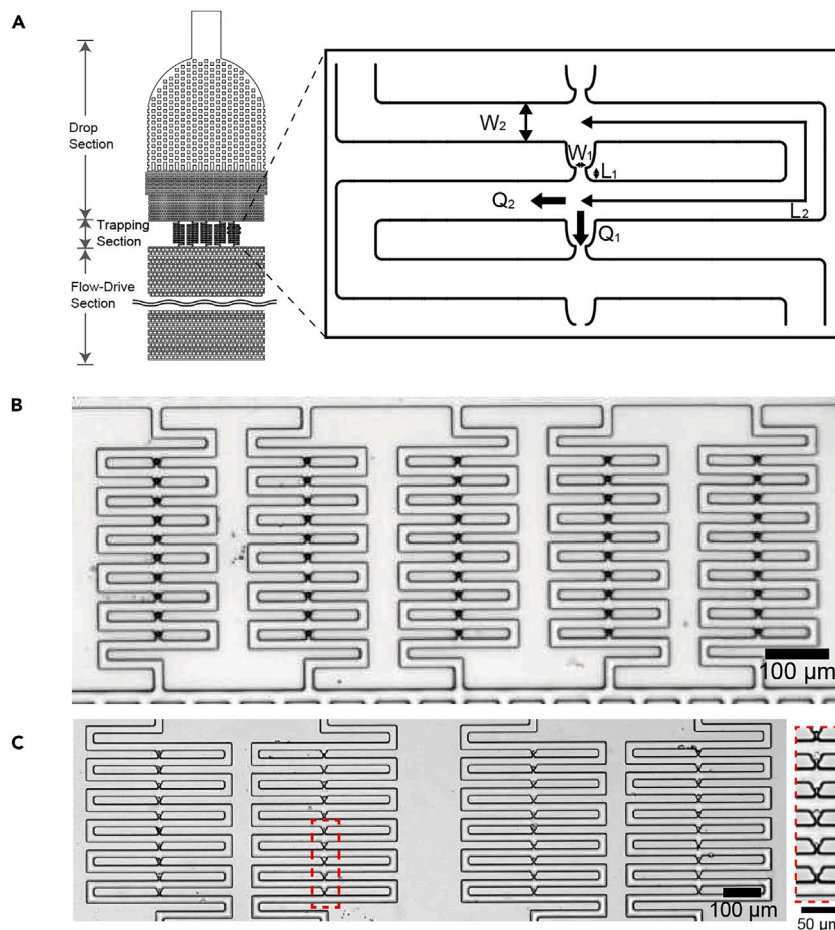


Figure 3. Design and trapping results in the open microchannel with Tan's architecture

(A) Design of the open microfluidic channel.

(B) Result of trapping 10 μm polystyrene microbeads at 50 trapping sites. $W_1 = 5$, $L_1 = 5$, $W_2 = 15$, $L_2 = 200$, and $H = 16$ μm .

(C) Result of trapping Jurkat cell at 40 trapping sites. $W_1 = 5$, $L_1 = 10$, $W_2 = 20$, $L_2 = 400$, and $H = 16$ μm . A close-up micrograph of cell trapping sites, which are marked with a dotted red line, is shown on the right.

Beads and cell trapping based on Tan's architecture

Next, we tested the hydrodynamic trapping of cell-sized particles and cells using the SCF in an open channel. First, we designed the deterministic trap channel based on that developed by Tan et al. in 2007¹⁷ (Figure 3A), which was placed at the channel section among the three sections shown in Figure 1B. In the drop section, the size and spacing of the pillars were reduced to separate the cells and filter out the cell aggregates before they entered the trapping (channel) section.

The dimensions of the trap channel were determined as follows: First, if the bypass channel width (W_2) is overly large, then the flow rate through the small gap in the trap (Q_1) decreases, which renders the trap inefficient. Furthermore, the narrower the bypass channel width, the more likely the occurrence of an SCF. Thus, W_2 should not be significantly larger than the size of the cells. Second, a larger channel height (H) is beneficial to the generation of SCF, as predicted theoretically and through preliminary experiments (Figure 2). By contrast, if H is overly large and exceeds the diameter of the cells, then multiple traps tend to occur in the depth direction of the trapping gap (Figure S5). Considering the results of the preliminary tests (Figure 2) and the points above, Tan's hydrodynamic trapping channel with an open architecture was fabricated with $H = 16$ μm , $W_2 = 15$ μm , and $L_2 = 200$ μm for trapping beads and cells measuring 10 μm in diameter. The width of the trapping gap W_1 was set to 5 μm (Figure 3A, right). In this device, Q_1/Q_2 was calculated as approximately 3.7. The traps were placed at 50 different locations.

First, the trapping of 10 μm beads was tested. A drop of 1% F-68 solution (0.5–1 μL) was deposited in the drop section such that the fluid was driven into and completely filled the channel section via SCF. This procedure, i.e., the filling of the cell-free solution, is recommended because the initial velocity of the solution when filling the dry channel is extremely high and makes cells pass through the trap. Stable flow at a relatively low velocity was achieved by initially applying the cell-free solution and then allowing the interface front to propagate at a constant velocity in the flow-drive section to drag the fluid into the trap section. After the channel section was filled with fluid, 1 μL of a 10.2 μm microbead solution at a concentration of $5 \times 10^5/\text{mL}$ diluted with 1%v/v F-68 solution was applied. The beads entered the channel

section stochastically from the drop section to be trapped. After 1–3 min, trapping at an efficiency of approximately 100% was achieved (Figure 3B; Video S3). Triplicate experiments resulted in 49.3 successful single-bead trapping among 50 traps, with a maximum rate of 100%. Factors contributing to some locations not being trapped included multiple beads being trapped in a single trap or debris or bead aggregates clogging the trap.

Next, we trapped the model cell (Jurkat cell; diameter: 10–15 μm). In this experiment, we modified the geometry of the trapping channel to reduce the flow velocity by widening and lengthening the bypass channel ($W_2 = 20 \mu\text{m}$ and $L_2 = 400 \mu\text{m}$, resulting in $Q_1/Q_2 \approx 1.8$). This was performed because, when we attempted to trap cells with a channel identical to that for beads, the cells tended to be squeezed into the trap and passed through it because of their deformability. Using the modified device, we achieved single-cell trapping at an efficiency of approximately 100% (Figure 3C; Video S4). The reason why we could not determine the absolute trapping efficiency was that, under bright field light microscopy, some trapped particles were difficult to judge if they were single cells or debris (e.g., the lowest trap within the inset marked by the red dotted rectangle). Nonetheless, the present open trapping device was confirmed to work similarly to that comprising the closed channel.

Beads and cell trapping and retrieval based on Chung's architecture

In the hydrodynamic trap channel of Tan's architecture,¹⁷ the traps were located at short distances. This design is suitable for dense arraying but not for the selection of individual cells. To enable single-cell picking from an open microfluidic cell array, the distance between neighboring trapping sites should be several times greater than the diameter of the pipette tip to avoid aspiration of multiple cells. Hence, we created a modified version of the trapping channel proposed by Chung et al. (2011)³³ (Figure S6A), which featured a distance of approximately 1 mm between neighboring trapping sites.

When the same channel geometry as in the study above was used, beads accumulated in the middle of a wide area within the channel (Figure S5B; Video S5). This occurred because a concave meniscus was formed at the edges and corners, which caused the liquid level to decrease toward the center of the channel. Thus, the beads were immobilized at a point where the water level was less than the diameter of the beads. Therefore, the wide section of the channel had to be partitioned into sections smaller than the capillary length of the solution such that the liquid surface remained almost flat at the top surface. The entire microfluidic design comprised three sections, similar to that used in previous experiments (Figure 4A), and the trap channels of Chung's architecture comprised channels partitioned with a width of 30 μm (Figure 4A, inset) inserted into the trapping section. Flow rate analysis using the equivalent electric circuit confirmed that the flow rate ratio required for trapping was maintained even though the paths separated into complex geometries (Figures S6C and S6D). When the bead solution ($5 \times 10^5/\text{mL}$ in 1%v/v F-68 aqueous solution) flowed through this channel, a single bead was successfully trapped in all 10 traps (Figures 4B and 4C; Video S6).

Similarly, we performed the same trapping experiment based on Jurkat cells using the same device and discovered that the cells were trapped at all 10 trapping sites (Figures 5A and 5B; Video S7). Although the frequency was low, some cells deformed or aggregated during trapping (Figure S7). However, this problem is not limited to open microfluidics but is characteristic of hydrodynamic cell trapping. Furthermore, it can be improved via pretreatment to improve cell uniformity and remove debris, or by embedding cells in gel microdroplets, if necessary.^{34–36}

Next, we attempted to capture the trapped cells via capillary suction. If the device remains exposed to air for a long duration (which depends on the atmosphere but is typically more than several minutes) then drying becomes problematic. Therefore, after confirming cell trapping under a microscope, the entire channel device was immersed in water in a dish with a diameter of 5 cm (Figure 5C). The cells and beads were retained in the trap when the device was gently immersed manually. During viewing under a microscope, a glass capillary with a tip diameter of 15 μm was shifted closer to the trapped cell using a micromanipulator and aspirated using a micro-aspiration pump. Subsequently, the aspirated cell was discharged into another container (Figure 5D; Video S8).

Because picking using manual micromanipulators is labor-intensive and time-consuming, a robotic picking machine (Spheroid Go, Aeternus, Japan) with positioning using a motorized XY stage was tested for picking trapped cells (Figure 5E). A glass capillary with a tip diameter of 30 μm was used. The capillary tip was viewed on a screen and positioned by specifying the suction spot while the trapped cells in the channel were observed with the zoom lens from the bottom. Furthermore, the capillary can discharge aspirated cells into a well plate placed on an adjacent stage. In this study, only the picking (aspiration) operation was performed to demonstrate the principle of single-cell trapping in an open trap and semi-automatic picking. After placing the trapping device on the stage of the robotic picking apparatus, Jurkat cell suspension was introduced into the drop region in the same manner as shown in Figure 5A. After the trapping was completed, cells were aspirated by clicking each trapped cell in the microscope image shown on the PC screen. Here, the z position of the capillary tip was found to be an important parameter for cell aspiration from the trap. In the conventional cell-picking method, in which cells are dispersed on a glass plate, the capillary tip position is typically set slightly above the cells (Figure S8A). However, in the present trapping device, the cells were placed below the top surface of the PDMS substrate, which did not result in successful cell acquisition (Figure S8B). Even when the tip position was set at the same height as the top surface of the substrate, the success rate of cell acquisition was relatively low (approximately 50%). When the capillary tip was set 100 μm below the top surface such that the tip was pressed against the PDMS (Figure S8C), the success rate of cell acquisition drastically increased. We speculate that, owing to the deformability of PDMS, this better aspiration yield was achieved because the capillary tip was set closer to the trapped cells. Under this setting, all trapped cells were successfully aspirated among 7, 7, and 9 trapped cells in the 10-trap device in triplicated experiments, resulting in a picking yield of 100% (Figure 5G; Video S9). The yields of single-cell trapping were not always 100% mainly because of the presence of aggregates of several cells and/or cell debris similarly to the experiment shown in Figure 3C. In

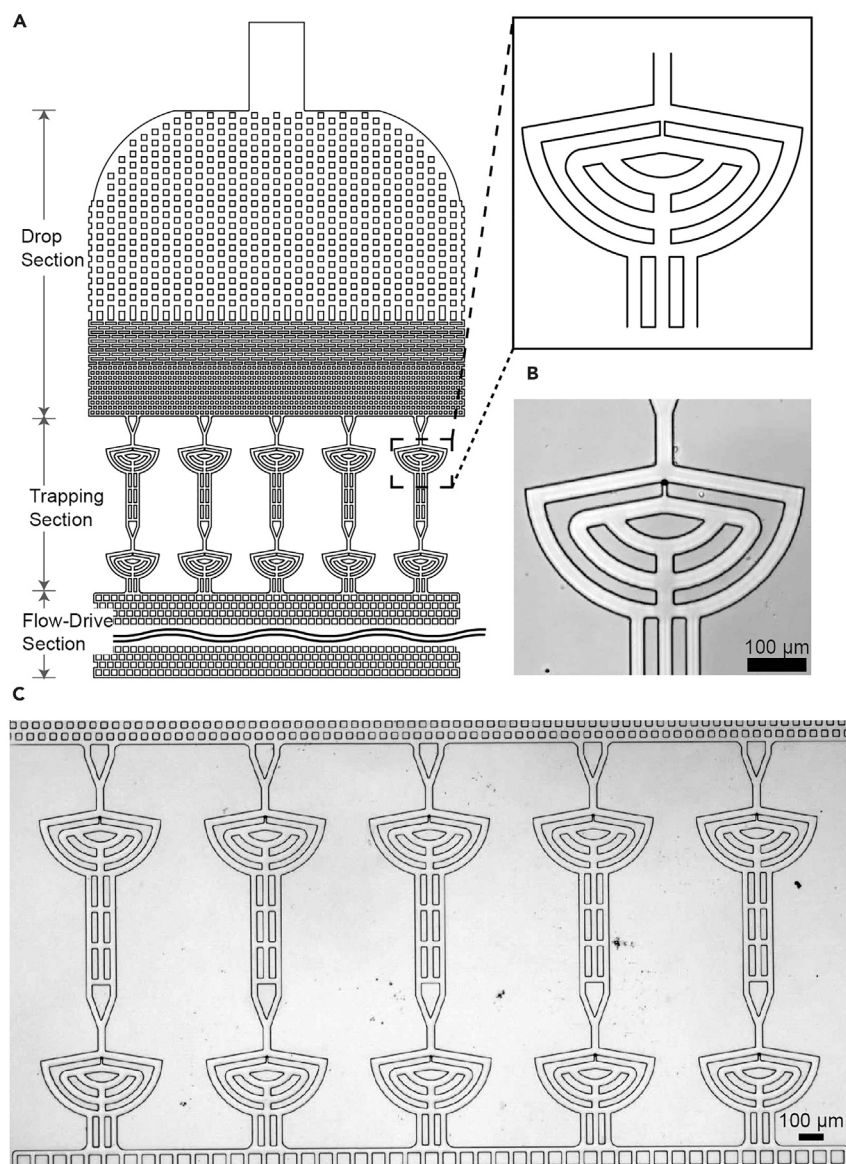


Figure 4. Design and trapping results in the open microchannel with modified Chung's architecture

(A) Design of the open microfluidic device. $W_2 = 30$ and $H = 16$ μm .

(B) Result of trapping 10 μm polystyrene microbeads at a single trapping site.

(C) Result of trapping 10 μm polystyrene microbeads at 10 trapping sites.

some cases (<10% of the trials), the cell squeezed into the trap required several aspirating trials, but eventually all trapped cells were successfully aspirated. In the future, this squeezing problem can be remedied by using softer channel material or partitioning the narrow trapping path.³⁷ This problem is not unique to open channels but is characteristic of deterministic hydrodynamic trapping. In this study, we successfully constructed a system in which capillaries for picking can be readily accessed via an open single-cell trapping microchannel.

DISCUSSION

In this study, we constructed a system in which an open microfluidic channel driven by an SCF was applied to hydrodynamic single-cell traps. Single-cell trapping requires fluid driving in a channel with a width and depth on the order of the cell size (10–50 μm). To realize a stable SCF in a semi-open channel on this scale, we established a protocol to hydrophilize only the inner walls of the channel and showed that treatment with F-68 surfactant was suitable. Using this system, we tested the well-established deterministic hydrodynamic trapping channels based on those developed by Tan et al. (2007)¹⁷ and Chung et al. (2011)³³ in an open-channel format. Results showed that similar

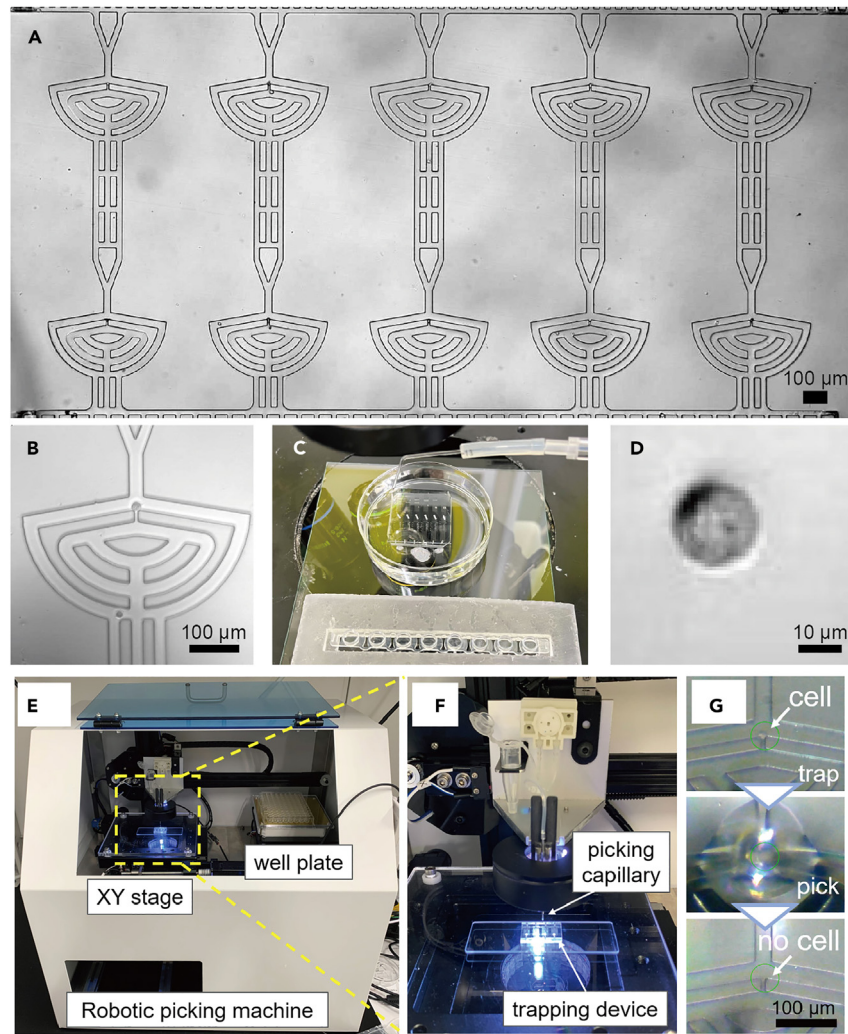


Figure 5. Retrieval of trapped cells

(A) Result of trapping Jurkat cell.

(B) Close-up view of a trapped cell.

(C) Overview of experimental setup for cell picking via capillary suction using a manual micromanipulator. The open channel was immersed in water after cell trapping was confirmed.

(D) Micrograph of a cell retrieved and transferred to another container.

(E) Overview of robotic picking machine equipped with a microscope and motorized XY stage.

(F) Close-up view of picking region. The trapping device was directly aspirated in the demonstration shown in Figure 5 because simple picking is fast and facile. However, it will take a much longer time to pick and transfer a larger number of cells. In such cases, drying of the fluid in the capillary could be a problem. We also confirmed that firmly trapped (squeezed) cells remained at trapping sites even when the entire device was immersed in a buffer in a dish (Figure S9; Video S10). Then, trapped cells can be aspirated with the same protocol. Finally, we emphasize that the present open-channel device is flexible in the sense that it is compatible with most of the deterministic hydrodynamic cell-trapping architectures,^{16,38–48} and the integration of additional components, such as electrodes, for *in situ* manipulation and analysis are also straightforward.^{49–51}

(G) Cell picking sequence.

trapping can be achieved using the same principle as the conventional closed channel to show the versatility of our open microfluidics architecture. The former is suitable for high-density arraying, whereas the latter, by increasing the distance between the traps, allows suction by capillaries with diameters ranging from several tens to hundreds of micrometers. Here, we designed the latter trapping channel to have a 1 mm distance between traps to allow aspiration with any capillary diameter, but traps could be placed with a higher density depending on the capillary size. With this device, we demonstrated that the integration of the system with a semi-automatic cell-picking robot is realizable. The trapped cells were directly aspirated in the demonstration shown in Figure 5 because simple picking is fast and facile. However, it will take a much longer time to pick and transfer a larger number of cells. In such cases, drying of the fluid in the capillary could be a problem. We also confirmed that firmly trapped (squeezed) cells remained at trapping sites even when the entire device was immersed in a buffer in a dish (Figure S9; Video S10). Then, trapped cells can be aspirated with the same protocol. Finally, we emphasize that the present open-channel device is flexible in the sense that it is compatible with most of the deterministic hydrodynamic cell-trapping architectures,^{16,38–48} and the integration of additional components, such as electrodes, for *in situ* manipulation and analysis are also straightforward.^{49–51}

In summary, open microfluidics is superior in bridging microfluidic devices and the existing macroscale apparatus used in conventional biology. The system can be extremely simple because the fluid is driven spontaneously without pumps and tubing. Picking cells from an array offers the following advantages over picking them from a flat substrate where cells are sparsely and randomly dispersed. (1) Because the position of cells on the chip is determined, positioning via image recognition is unnecessary or simplified. (2) The risk of accidental drawing of nearby cells is absent. (3) In single-cell analysis such as scRNA-seq, the presence or absence of cells using images can be confirmed, and the correlation between cell morphology and gene expression patterns can be examined.⁵² The present technology is expected to expand the applications of single-cell analysis protocols used in various fields such as pharmaceuticals, diagnosis, healthcare, and life science.

Limitations of the study

The following issues remain to be resolved. First, in the present microchannel design, cells remained in the drop section and the flow-driving section was not used, which decreases the trapping efficiency relative to the entire cell population. However, this is not a significant disadvantage compared with using closed microchannel systems that require dead volume in the tubing. Second, SCF will stop when all of the flow paths are filled with fluid. However, the flow could be continued or re-started if the fluid is soaked from the downstream, e.g., by applying a filter paper.

Our next challenge is to expand the present system to create large arrays. The flow path inevitably becomes sufficiently long to increase the number of traps. However, SCF is driven by the wetting and spreading of the progressing front of the water interface, and the longer the length of the channel trailing behind it, the slower is the progression because of the increased viscous drag. Consequently, a longer time is required and more drying occurs, which necessitates trapping under strict humidity-controlled conditions. Therefore, the lengths of all trapping sections were designed to be less than 1 cm in this study. If this length is increased 10-fold, then the problems above must be considered. One possible solution is to introduce trapping and flow-driving sections alternately. Another issue is the improvement in the accuracy of single-cell trapping. Conventional closed-channel hydrodynamic trapping devices can easily trap highly uniform and robust particles, such as microbeads; however, single-cell trapping becomes less efficient because of the significant size variation, deformability, and presence of debris. In addition, a problem specific to cell picking from an open-channel trap is that a certain percentage of cells are soft and difficult to aspirate if they are pushed deeply into the trap. These issues require further detailed study, such as the use of softer PDMS substrates or the design of easily deformable trap structures.

STAR★METHODS

Detailed methods are provided in the online version of this paper and include the following:

- KEY RESOURCES TABLE
- RESOURCE AVAILABILITY
 - Lead contact
 - Materials availability
 - Data and code availability
- METHOD DETAILS
 - Device fabrication
 - Cell culture

SUPPLEMENTAL INFORMATION

Supplemental information can be found online at <https://doi.org/10.1016/j.isci.2023.108323>.

ACKNOWLEDGMENTS

This study was performed in collaboration with On-chip Biotechnologies Co., Ltd. and Aeternus Co., Ltd., and was supported by JSPS Grant-in-Aids (19H05626, 19H02576, and 20H05935), Japan Keirin Autorace foundation (JKA), and the Institute of Science and Engineering at the Chuo University.

AUTHOR CONTRIBUTIONS

T.M. and H.S. conceived of the project. T.M. designed and fabricated the device and performed most of the experiments. M.T. prepared cells. H.T. performed the contact angle measurements and device fabrication for the automated picking experiments. H.T., M.N., and D.A. conducted the automated picking experiments. T.M. and H.S. wrote the manuscript. All authors have reviewed the manuscript and approved the final article.

DECLARATION OF INTERESTS

We have no financial interest to declare.

H.S. and T.M. are inventors of a pending patent (Japanese Patent application No. 2022-076712), which covers the fabrication method and design of open microchannel for cell/particle trapping introduced in this article.

Received: March 13, 2023
Revised: September 28, 2023
Accepted: October 20, 2023
Published: October 24, 2023

REFERENCES

- Wang, D., and Bodovitz, S. (2010). Single cell analysis: the new frontier in 'omics'. *Trends Biotechnol.* 28, 281–290. <https://doi.org/10.1016/j.tibtech.2010.03.002>.
- Stuart, T., and Satija, R. (2019). Integrative single-cell analysis. *Nat. Rev. Genet.* 20, 257–272. <https://doi.org/10.1038/s41576-019-0093-7>.
- Wang, Y., and Navin, N.E. (2015). Advances and applications of single-cell sequencing technologies. *Mol. Cell* 58, 598–609. <https://doi.org/10.1016/j.molcel.2015.05.005>.
- Salomon, R., Kaczorowski, D., Valdes-Mora, F., Nordon, R.E., Neild, A., Farbehni, N., Bartonicek, N., and Gallego-Ortega, D. (2019). Droplet-based single cell RNAseq tools: a practical guide. *Lab Chip* 19, 1706–1727. <https://doi.org/10.1039/c8lc01239c>.
- Chen, W., Li, S., Kulkarni, A.S., Huang, L., Cao, J., Qian, K., and Wan, J. (2020). Single cell omics: From assay design to biomedical application. *Biotechnol. J.* 15, e1900262. <https://doi.org/10.1002/biot.201900262>.
- Liu, D., Sun, M., Zhang, J., Hu, R., Fu, W., Xuanyuan, T., and Liu, W. (2022). Single-cell droplet microfluidics for biomedical applications. *Analyst* 147, 2294–2316. <https://doi.org/10.1039/d1an02321g>.
- Lin, C.H., Hsiao, Y.H., Chang, H.C., Yeh, C.F., He, C.K., Salm, E.M., Chen, C., Chiu, I.M., and Hsu, C.H. (2015). A microfluidic dual-well device for high-throughput single-cell capture and culture. *Lab Chip* 15, 2928–2938. <https://doi.org/10.1039/c5lc00541h>.
- Swennenhuis, J.F., Tibbe, A.G.J., Stevens, M., Katika, M.R., van Dalum, J., Tong, H.D., van Rijn, C.J.M., and Terstappen, L.W.M.M. (2015). Self-seeding microwell chip for the isolation and characterization of single cells. *Lab Chip* 15, 3039–3046. <https://doi.org/10.1039/c5lc00304k>.
- Chin, V.I., Taupin, P., Sanga, S., Scheel, J., Gage, F.H., and Bhatia, S.N. (2004). Microfabricated platform for studying stem cell fates. *Biotechnol. Bioeng.* 88, 399–415. <https://doi.org/10.1002/bit.20254>.
- Rettig, J.R., and Folch, A. (2005). Large-scale single-cell trapping and imaging using microwell arrays. *Anal. Chem.* 77, 5628–5634. <https://doi.org/10.1021/ac0505977>.
- Yoshimoto, N., Kida, A., Jie, X., Kurokawa, M., Iijima, M., Niimi, T., Maturana, A.D., Nikaido, I., Ueda, H.R., Tatematsu, K., et al. (2013). An automated system for high-throughput single cell-based breeding. *Sci. Rep.* 3, 1191. <https://doi.org/10.1038/srep01191>.
- Yoshimoto, N., and Kuroda, S. (2014). Single-cell-based breeding: Rational strategy for the establishment of cell lines from a single cell with the most favorable properties. *J. Biosci. Bioeng.* 117, 394–400. <https://doi.org/10.1016/j.jbiosc.2013.09.016>.
- Narayanamurthy, V., Nagarajan, S., Firus Khan, A.Y., Samsuri, F., and Sridhar, T.M. (2017). Microfluidic hydrodynamic trapping for single cell analysis: mechanisms, methods and applications. *Anal. Methods* 9, 3751–3772. <https://doi.org/10.1039/c7ay00656j>.
- Luan, Q., Macaraniag, C., Zhou, J., and Papautsky, I. (2020). Microfluidic systems for hydrodynamic trapping of cells and clusters. *Biomicrofluidics* 14, 031502. <https://doi.org/10.1063/5.0002866>.
- Deng, Y.L., Guo, Y., and Xu, B. (2020). Recent Development of Microfluidic Technology for Cell Trapping in Single Cell Analysis: A Review. *Processes* 8, 1253. <https://doi.org/10.3390/pr8101253>.
- Di Carlo, D., Wu, L.Y., and Lee, L.P. (2006). Dynamic single cell culture array. *Lab Chip* 6, 1445–1449. <https://doi.org/10.1039/b605937f>.
- Tan, W.H., and Takeuchi, S. (2007). A trap-and-release integrated microfluidic system for dynamic microarray applications. *Proc. Natl. Acad. Sci. USA* 104, 1146–1151. <https://doi.org/10.1073/pnas.0606625104>.
- Zhong, J.F., Chen, Y., Marcus, J.S., Scherer, A., Quake, S.R., Taylor, C.R., and Weiner, L.P. (2008). A microfluidic processor for gene expression profiling of single human embryonic stem cells. *Lab Chip* 8, 68–74. <https://doi.org/10.1039/b712116d>.
- Kaigala, G.V., Lovchik, R.D., and Delamarche, E. (2012). Microfluidics in the "open space" for performing localized chemistry on biological interfaces. *Angew. Chem. Int. Ed.* 51, 11224–11240. <https://doi.org/10.1002/anie.201201798>.
- Berthier, E., Dostie, A.M., Lee, U.N., Berthier, J., and Theberge, A.B. (2019). Open microfluidic capillary systems. *Anal. Chem.* 91, 8739–8750. <https://doi.org/10.1021/acs.analchem.9b01429>.
- Zhang, Q., Feng, S., Lin, L., Mao, S., and Lin, J.M. (2021). Emerging open microfluidics for cell manipulation. *Chem. Soc. Rev.* 50, 5333–5348. <https://doi.org/10.1039/d0cs01516d>.
- Berthier, J., Brakke, K.A., and Berthier, E. (2014). A general condition for spontaneous capillary flow in uniform cross-section microchannels. *Microfluid. Nanofluid.* 16, 779–785. <https://doi.org/10.1007/s10404-013-1270-1>.
- Berthier, J., Gosselin, D., and Berthier, E. (2015). A generalization of the Lucas-Washburn-Rideal law to composite microchannels of arbitrary cross section. *Microfluid. Nanofluid.* 19, 497–507. <https://doi.org/10.1007/s10404-014-1519-3>.
- Tan, J.N., Alan, T., and Neild, A. (2013). Stability of flowing open fluidic channels. *AIP Adv.* 3, 022121. <https://doi.org/10.1063/1.4792940>.
- Berthier, J., Brakke, K.A., Furlani, E.P., Karampelas, I.H., Poher, V., Gosselin, D., Cubizolles, M., and Pouteau, P. (2015). Whole blood spontaneous capillary flow in narrow V-groove microchannels. *Sens. Act. B: Chemical* 206, 258–267. <https://doi.org/10.1016/j.snb.2014.09.040>.
- Berthier, J., Brakke, K.A., Gosselin, D., Navarro, F., Belgacem, N., and Chaussy, D. (2016). Spontaneous capillary flow in curved, open microchannels. *Microfluid. Nanofluid.* 20, 100. <https://doi.org/10.1007/s10404-016-1766-6>.
- Tran, T.S.H., Ho, B.D., Beech, J.P., and Teegenfeldt, J.O. (2017). Open channel deterministic lateral displacement for particle and cell sorting. *Lab Chip* 17, 3592–3600. <https://doi.org/10.1039/c7lc00707h>.
- Masuda, T., Song, W., Nakanishi, H., Lei, W., Noor, A.M., and Arai, F. (2017). Rare cell isolation and recovery on open-channel microfluidic chip. *PLoS One* 12, e0174937. <https://doi.org/10.1371/journal.pone.0174937>.
- Wu, Z., and Hjort, K. (2009). Surface modification of PDMS by gradient-induced migration of embedded Pluronic. *Lab Chip* 9, 1500–1503. <https://doi.org/10.1039/b901651a>.
- Trantidou, T., Elani, Y., Parsons, E., and Ces, O. (2017). Hydrophilic surface modification of PDMS for droplet microfluidics using a simple, quick, and robust method via PVA deposition. *Microsyst. Nanoeng.* 3, 16091. <https://doi.org/10.1038/micronano.2016.16091>.
- Azizpour, N., Avazpour, R., Sawan, M., Rosenzweig, D.H., and Ajji, A. (2022). Uniformity of spheroids-on-a-chip by surface treatment of PDMS microfluidic platforms. *Sens. Diagn.* 1, 750–764. <https://doi.org/10.1039/d2sd00004k>.
- Xu, X., and Wang, X. (2020). Theoretical analysis for dynamic contact angle hysteresis on chemically patterned surfaces. *Phys. Fluids* 32, 112102. <https://doi.org/10.1063/5.0027747>.
- Chung, J., Kim, Y.J., and Yoon, E. (2011). Highly-efficient single-cell capture in microfluidic array chips using differential hydrodynamic guiding structures. *Appl. Phys. Lett.* 98, 123701. <https://doi.org/10.1063/1.3565236>.
- Manome, A., Zhang, H., Tani, Y., Katsuragi, T., Kurane, R., and Tsuchida, T. (2001). Application of gel microdroplet and flow cytometry techniques to selective enrichment of non-growing bacterial cells. *FEMS Microbiol. Lett.* 197, 29–33.
- Hosokawa, M., Hoshino, Y., Nishikawa, Y., Hirose, T., Yoon, D.H., Mori, T., Sekiguchi, T., Shoji, S., and Takeyama, H. (2015). Droplet-based microfluidics for high-throughput screening of a metagenomic library for isolation of microbial enzymes. *Biosens. Bioelectron.* 67, 379–385. <https://doi.org/10.1016/j.bios.2014.08.059>.
- Sun, H., Hu, N., and Wang, J. (2022). Application of microfluidic technology in antibody screening. *Biotechnol. J.* 17, e2100623. <https://doi.org/10.1002/biot.202100623>.
- Kumano, I., Hosoda, K., Suzuki, H., Hirata, K., and Yomo, T. (2012). Hydrodynamic trapping of *Tetrahymena thermophila* for the long-term monitoring of cell behaviors. *Lab Chip* 12, 3451–3457. <https://doi.org/10.1039/c2lc40367f>.
- Faley, S., Seale, K., Hughey, J., Schaffer, D.K., VanCompernelle, S., McKinney, B., Baudenbacher, F., Unutmaz, D., and Wiksw, J.P. (2008). Microfluidic platform for real-time

- signaling analysis of multiple single T cells in parallel. *Lab Chip* 8, 1700–1712. <https://doi.org/10.1039/b719799c>.
39. Arakawa, T., Noguchi, M., Sumitomo, K., Yamaguchi, Y., and Shoji, S. (2011). High-throughput single-cell manipulation system for a large number of target cells. *Biomicrofluidics* 5, 14114. <https://doi.org/10.1063/1.3567101>.
 40. Chung, K., Rivet, C.A., Kemp, M.L., and Lu, H. (2011). Imaging single-cell signaling dynamics with a deterministic high-density single-cell trap array. *Anal. Chem.* 83, 7044–7052. <https://doi.org/10.1021/ac2011153>.
 41. Kim, J., Erath, J., Rodriguez, A., and Yang, C. (2014). A high-efficiency microfluidic device for size-selective trapping and sorting. *Lab Chip* 14, 2480–2490. <https://doi.org/10.1039/c4lc00219a>.
 42. Sarioglu, A.F., Aceto, N., Kojic, N., Donaldson, M.C., Zeinali, M., Hamza, B., Engstrom, A., Zhu, H., Sundaresan, T.K., Miyamoto, D.T., et al. (2015). A microfluidic device for label-free, physical capture of circulating tumor cell clusters. *Nat. Methods* 12, 685–691. <https://doi.org/10.1038/Nmeth.3404>.
 43. Jin, D., Deng, B., Li, J.X., Cai, W., Tu, L., Chen, J., Wu, Q., and Wang, W.H. (2015). A microfluidic device enabling high-efficiency single cell trapping. *Biomicrofluidics* 9, 014101. <https://doi.org/10.1063/1.4905428>.
 44. Wang, Y., Tang, X., Feng, X., Liu, C., Chen, P., Chen, D., and Liu, B.F. (2015). A microfluidic digital single-cell assay for the evaluation of anticancer drugs. *Anal. Bioanal. Chem.* 407, 1139–1148. <https://doi.org/10.1007/s00216-014-8325-3>.
 45. Mi, L., Huang, L., Li, J., Xu, G., Wu, Q., and Wang, W. (2016). A fluidic circuit based, high-efficiency and large-scale single cell trap. *Lab Chip* 16, 4507–4511. <https://doi.org/10.1039/c6lc01120a>.
 46. Weng, L., Ellett, F., Edd, J., Wong, K.H.K., Uygun, K., Irimia, D., Stott, S.L., and Toner, M. (2017). A highly-occupied, single-cell trapping microarray for determination of cell membrane permeability. *Lab Chip* 17, 4077–4088. <https://doi.org/10.1039/c7lc00883j>.
 47. Zhou, J., Tu, C., Liang, Y., Huang, B., Fang, Y., Liang, X., and Ye, X. (2020). The label-free separation and culture of tumor cells in a microfluidic biochip. *Analyst* 145, 1706–1715. <https://doi.org/10.1039/c9an02092f>.
 48. Weng, L., Ellett, F., Edd, J., Wong, K.H.K., Uygun, K., Irimia, D., Stott, S.L., and Toner, M. (2017). A highly-occupied, single-cell trapping microarray for determination of cell membrane permeability. *Lab Chip* 17, 4077–4088. <https://doi.org/10.1039/C7LC00883J>.
 49. Kim, S.H., Yamamoto, T., Fourmy, D., and Fujii, T. (2011). Electroactive microwell arrays for highly efficient single-cell trapping and analysis. *Small* 7, 3239–3247. <https://doi.org/10.1002/sml.201101028>.
 50. Wu, Y.C., Wu, T.H., Clemens, D.L., Lee, B.Y., Wen, X., Horwitz, M.A., Teitell, M.A., and Chiou, P.Y. (2015). Massively parallel delivery of large cargo into mammalian cells with light pulses. *Nat. Methods* 12, 439–444. <https://doi.org/10.1038/nmeth.3357>.
 51. Wang, J., Trouillon, R., Dunevall, J., and Ewing, A.G. (2014). Spatial resolution of single-cell exocytosis by microwell-based individually addressable thin film ultramicroelectrode arrays. *Anal. Chem.* 86, 4515–4520. <https://doi.org/10.1021/ac500443q>.
 52. Jin, J., Ogawa, T., Hojo, N., Kryukov, K., Shimizu, K., Ikawa, T., Imanishi, T., Okazaki, T., and Shiroguchi, K. (2023). Robotic data acquisition with deep learning enables cell image-based prediction of transcriptomic phenotypes. *Proc. Natl. Acad. Sci. USA* 120, e2210283120. <https://doi.org/10.1073/pnas.2210283120>.

STAR★METHODS

KEY RESOURCES TABLE

REAGENT or RESOURCE	SOURCE	IDENTIFIER
Chemicals, cells, and other consumables		
PDMS	Dow Corning Corp., USA	Sylgard-184
Negative photoresist	Nippon Kayaku, Co. Ltd., Japan	SU-8 3010
2inch one-side polished silicon wafer	Matsuzaki Seisakusyo Co., Ltd., Japan	<100 > t = 300μm
10.2 μm polystyrene beads	Spherotech, Inc., USA	PPS-4
Jurkat Cell	Japanese Collection of Research Bioresources Cell Bank	
Pluronic F-68	Thermo Fisher Scientific Inc., USA	24040032
Polyvinyl alcohol (PVA)	Sigma Aldrich (Merck KGaA)	363170-25G
Sucrose	Sigma Aldrich (Merck KGaA)	S0389-500G
RPMI-1640 Medium	Wako, Japan	189-02025
Fetal Bovine Serum (FBS)	Hyclone	SH30910.03
Software		
Fiji (ImageJ)	NIH	
Other		
Compact etcher (Oxygen plasma)	Samco Inc., Japan	FA-1
High-speed camera	Teledyne FLIR LLC, USA	GS3-U3-23S6M-C
Microscope	Olympus, Japan	IX51
Automated cell-picking apparatus	Aeternus Co., Ltd., Japan	Spheroid Go
Nanoliter suction device	Nepa Gene Co., Ltd, Japan	PicoPipet
L-shaped glass capillary	Nepa Gene Co., Ltd, Japan	1-GS15L-10

RESOURCE AVAILABILITY

Lead contact

Requests for additional information and resources should be directed to the lead contact, Hiroaki Suzuki (suzuki@mech.chuo-u.ac.jp).

Materials availability

The design of microfluidic devices fabricated for this study may be available by contacting the [lead contact](#).

Data and code availability

All data reported in this paper will be shared by the lead contact upon request. This paper does not report original code.

METHOD DETAILS

Device fabrication

The PDMS open microchannel was designed using CAD software (Rhino 6.0) and fabricated as follows:

- (1) A master mold with a height of 16 μm was fabricated using a negative photoresist (SU-8 3010, Microchem) on a 2-inch silicon wafer via photolithography based on the manufacturer's protocol.
- (2) PDMS resin (Sylgard-184, Dow Corning) mixed with its curing agent at a 10:1 wt ratio was poured into the master mold.
- (3) After curing at 80°C for 120 min, the PDMS slab was peeled off from the mold.
- (4) After removing undesired portions using a surgical knife, 0.75 mm holes were created as the inlet and outlet of the flow path.
- (5) Steps (2) and (3) were prepared to prepare a flat PDMS (without structure).
- (6) Oxygen plasma was applied to the channel side surface of the PDMS microchannel using a compact etcher (O₂ flow rate: 20 mL/min, 75 W) for 5 s.

- (7) A flat PDMS was placed on the channel surface of the PDMS device and pressed gently with a finger until air was removed. Subsequently, a drop of 1%v/v F-68 solution was deposited into the inlet hole to fill the channel for approximately 30 min.
- (9) A tube was inserted at the inlet or outlet holes to apply negative pressure such that the F-68 solution was removed completely from the microchannel.
- (10) The flat PDMS was peeled off, and the PDMS device with the transferred structure face down (facing the hot plate face) was baked on a hot plate at 120°C for 10–20 min.
- (11) The hole at the inlet of the flow channel was covered with another flat PDMS.
- (12) A drop of solution was deposited into the drop section for the SCF and trapping experiments.

Cell culture

Jurkat cells (Japanese Collection of Research Bioresources Cell Bank) were cultured in an RPMI-1640 medium (Sigma–Aldrich) supplemented with 10% fetal bovine serum (Life Technologies) and penicillin/streptomycin (50 U ml⁻¹; Sigma–) at 37°C in 5% CO₂. The cells were resuspended in a buffer comprising 130 mM NaCl, 5.4 mM KCl, 1.8 mM CaCl₂, 0.8 mM MgCl₂, 5.5 mM glucose, and 10 mM HEPES-NaOH (pH 7.3). The density of the cells was adjusted to $\sim 1.0 \times 10^5$ cell/mL before they were applied to the open-channel trapping device.